Light Metals 2007 Edited by Morten Sørlie **TMS (The Minerals, Metals & Materials Society), 2007**

EFFICIENT OPERATION OF COMPRESSED AIR JETS FOR SIDEWALL COOLING

Robert J. Wallace[1], Mark P. Taylor[1], John J. J. Chen[2], Mohammed M. Farid[2]

[1]Light Metals Research Centre - The University of Auckland, Auckland, New Zealand
[2]Chemical and Materials Engineering Department- The University of Auckland, Auckland, New Zealand

Keywords: Sidewall cooling, nozzle, compressed air, jet

Abstract

Compressed air jets are commonly used for localised cooling of aluminium reduction cell sidewalls when process excursions occur or when sidewall tap outs are imminent. Typically compressed air is applied to cell sidewalls with large variation in the location and direction of air jets. Air flow consumption is generally high as full plant air pressure is used. Compressed air is expensive and has finite capacity hence its use for cooling should be efficient whilst being effective in prolonging cell lives. A range of experiments were conducted to explore the effects of supply air pressure, Reynolds number, jet to sidewall spacing and jet angle on sidewall heat transfer. The experiments were conducted at the Light Metals Research Centre - University of Auckland using a nominal half scale test rig representing cell sidewalls. This paper shows the importance of air pressure, Reynolds number, jet to sidewall distance, and jet angle on sidewall cooling.

Introduction

Compressed air jets are used within the aluminium smelting industry to locally cool hot regions of cell sidewalls. Compressed air jets, formed by supply compressed air to nozzles, are used as a preventative response to restore the protective sidewall ledge and prevent cell failure.

Sidewall cooling is becoming more important as cell energy intensification increases. To increase the capital return of existing assets, including the latest generation of high current cells, aluminium smelters throughout the world have increased line amperage over the last 15 years. Line amperage increases require cell heat balance modification to maintain stable cell operation and the protective sidewall ledge. Silicon carbide sidewall linings, graphatized cathodes and metal level alterations have all assisted in achieving adequate cell heat balance however these methods are reaching limits. The largest thermal resistance is now the overall heat transfer coefficient at the shell exterior. Air jet cooling, using either high pressure or low pressure air, can enhance heat transfer at the sidewall and is now being considered for continual use as demonstrated by Alcan-Pechiney's patented low pressure air jet cooling system [1] for high current cells.

Supplying compressed air to jet cooling systems is expensive especially at high pressure. Figure 1 shows

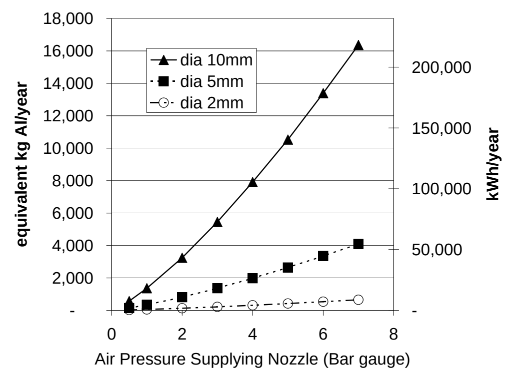

Figure 1: Energy requirement per year to provide compressed air to a single round nozzle at various supply pressures

the energy requirement per year, in both kWh and equivalent kilograms of aluminium production loss, to provide compressed air to a single round nozzle having either 2, 5 or 10mm outlet diameter over a range of supply air pressures. The calculations assume continuous air jet operation, 100% nozzle efficiency and air power calculated using equations for isothermal air compression as detailed in Kempes Engineers Year Book [2]. An aluminium energy conversion rate of 13.5 AC kWhr/kg was used.

Effective and efficient use of air jets requires an understanding of the effect of each nozzle arrangement factor on heat transfer; factors include: nozzle size, nozzle Reynolds number, air density at the nozzle exit (pressure dependant), impingement angle and the relative distance of the nozzle from the sidewall.

Literature

A large number of studies have been reported in the literature for impinging jet cooling. An early review paper by Martin [3] provides a comprehensive overview of impinging jet flow and factors that effect heat transfer. Martin defines three flow regions; free jet, stagnation and wall jet (flow) regions. The free jet is where the jet flow core velocity develops and extends from the nozzle exit to the stagnation region. The stagnation region is where the jet core velocity reduces from the free jet velocity to zero at the impinged surface and turns the flow parallel to the surface. The wall jet region is where the fluid flow is parallel to the impinged surface. Martin's [3] review paper includes a Nusselt number (Nu) correlation for a rectangular single slot nozzle geometrically defined by its slot width (B)and slot length (L). The slot length (L) is the full width of the impinged surface and arranged transversely to its longitudinal axis. The Nu correlation, applicable for both stagnation and wall jet regions, has factors; Reynolds number (Re), nozzle to surface distance (s/Dh), distance from stagnation point (x/Dh) and Prandtl number. Martin's Nu correlation generally shows reducing Nu with increasing s/Dh however it can result in a peak Nu in the stagnation region with increasing s/Dh depending on the combination of nozzle arrangement factors. Martin [3] also concludes the mean heat transfer is independent of impingement angle however the point of maximum heat transfer moves with impingement angle.

Beitelmal et al [4, 5] describe experiments of a rectangular single slot nozzle, arranged vertically and impinging down onto a uniformly heated (fixed heat flux) plate at various impingement angles. As in Martin [3] the slot length is the full width of the plate. Nu correlations were established for the stagnation, uphill and down hill wall jet regions and included the factors; Re, x/Dh, s/Dh and impingement angle. The correlations suggest reduced heat transfer with increased s/Dh distance (in contrast with Martin [3]), nozzle angle and increased heat transfer with Re.

Jambunathan et al's [6] review paper of single round nozzles reaffirms the primary factors of Martin's [3] Nu correlation and concludes that consideration of the following factors is also required; nozzle geometry, confinement and upstream turbulence of the flow to the nozzle. They also conclude that square edge nozzles give higher heat transfer than ASME elliptical nozzles at s/Dh $<$ 10.

Goldstein et al [7] conducted round nozzle experiments using impinging compressed air jets and showed that local Nu in the wall jet region is independent of s/Dh however in the stagnation region Nu_{stag} is dependant on s/Dh. The maximum Nu_{stag} occurred at s/Dh = 8 and is attributed to turbulent induced mixing of the jet stream.

Goldstein and Behbahani [8] explored the effect of cross flow velocities on round jet nozzles using compressed air and concluded that the maximum Nu reduces with increasing cross flow velocity at nozzle to surface spacing s/Dh = 12 however at s/Dh = 6 moderate cross flow increased the maximum Nu.

Rectangular single slot nozzles that cover the full width of the impinged surface may have different characteristics than a slot nozzle having a small slot length relative to the impinged surface width. Conditions typically found at the reduction cell sidewall are also different to those used in the literature including; vertical surface with turbulent natural convection transverse to the jet, significant thermal radiation from the sidewall to the nozzle, unique sidewall thermal profile and large heat fluxes (8-12kW/m^2 c.w. 3.95 kW/m^2 in [5]).

Experimental

Three different nozzle designs were tested on a half scale test rig representing the sidewalls of two aluminium reduction cells arranged side by side; the test rig is three cradles long. Each sidewall is heated by 12 - 750 Watt elements, oriented horizontally, stacked vertically and switched on and off by PLC controlled solid state relays to produce a sidewall temperature profile similar to that observed on actual cells; constant power input mode was used for the experiments. Test rig sidewall temperatures were measured using K type thermocouples embedded in the wall. Heat flux was measured using a HT50 heat flux sensor located at the jet impingement point. The locations of thermocouples, heat flux sensor and nozzle angles are shown in Figure 2.

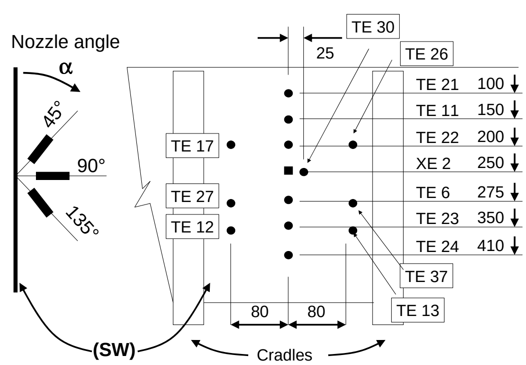

Figure 2: Nozzle angle (α) and location of thermocouples and heat flux sensor (XE2) on sidewall (SW)

Each experimental run consisted of applying a nozzle of a given size to the sidewall at a given angle and distance from sidewall; the nozzle impingement point was 250mm from the top of the sidewall, directly inline with the heat flux sensor (XE2). The 12.5mm nozzle was supplied with compressed air whilst the 20 and 40mm nozzles were supplied with low pressure air from a centrifugal blower. Nominal compressed air pressures of 0.8, 3.0 and 4.8 bar (gauge) were used for the 12.5mm nozzle, fan pressures (gauge) of 275, 515 and 1050 Pa for the 20mm nozzle and 65, 130 and 250 Pa for the 40mm nozzle were used.

The test rig was heated to steady state with no flow to the nozzle; temperatures and heat flux data were recorded. Air flow was applied to the nozzle to achieve a specified Reynolds number based on nozzle stagnation pressure and temperature. The test rig was allowed to reach steady state after which temperatures, heat flux and nozzle pressures were recorded. The process was repeated to achieve three different Reynolds numbers each day.

Three mean measures were calculated from the collected data. $T_{avg\ grid}$ represents the mean sidewall temperature and is the mean of temperature locations TE17, 27, 12, 22, 6, 23, 26, 37 and 13. $T_{avg\ grid}$ covers the central half width between cradles. $T_{avg\ profile}$ is the mean of temperatures located on the vertical centreline between shell cradles at locations TE21, 11, 22, 6, 23, 24. $U_{stag\ isen}$ is the overall heat transfer coefficient in the stagnation region and includes thermal radiation. $U_{stag\ isen}$ was calculated from the heat flux data (XE2), local sidewall temperature (TE6, 30) and the nozzle throat temperature (T_{throat}) using the following equations:

$$U_{stag\ isen} = \frac{q}{(T_w - T_{throat})} \tag{1}$$

$$T_w = \left(\frac{TE6 + TE30}{2}\right) \tag{2}$$

$$T_{throat} = T_o \left(\frac{P_{throat}}{P_o}\right)^{\frac{1.4-1}{1.4}} \tag{3}$$

$$P_{throat-unchoked} = P_{ambient} \tag{4}$$

$$P_{throat-choked} = 0.52828 P_o \tag{5}$$

Isentropic Reynolds number (Re_{isen}) was calculated from the measured nozzle stagnation pressure and temperature immediately upstream from the nozzle exit as follows:

$$Re_{isen} = \frac{uDh}{\nu} \tag{6}$$

$$u_{un\ chocked} = \left\{\frac{2\gamma RT}{\gamma - 1}\left[1 - \left(\frac{P_t}{P_o}\right)^{\frac{\gamma-1}{\gamma}}\right]\right\}^{\frac{1}{2}} \tag{7}$$

$$u_{chocked} = \left\{\frac{2\gamma RT}{\gamma + 1}\right\}^{\frac{1}{2}} \tag{8}$$

The equations above (equations 1 - 8)are from Zucrow and Hoffman [9] and assume ideal gas laws and isentropic flow. The critical pressure ratio determined whether choked or non choked flow equation for velocity was used.

Friction will cause non-isentropic flow within the nozzle resulting in a reduction of exit velocity hence the calculated Reynolds number assuming isentropic flow (Re_{isen}) will be higher than the true Reynolds number. Measuring the actual flow conditions at the nozzle exit is difficult, especially at the high temperatures found at the sidewall. Re_{isen} provides a robust method of determining nozzle flow conditions that can be replicated within the potroom environment allowing comparison of this experimental work with plant trials.

Two experimental sets were conducted in this work:

1. A factorial experiment, at low pressure, of the nozzle arrangement factors as follows:

Nozzle Size	12.5mm	20mm	40mm
Angle	45°	90°	135°
Re	4500	6500	9500
s/Dh	3	6	

2. A set of nozzle to wall distance (s/Dh) experiments with each nozzle at 90°

Nozzle design Nozzles were constructed by squashing the end of tubes to create a slot of specified width (dimension B) as shown in Figure 3. A tube enclosing a thermocouple is also shown which was used to measure stagnation pressure and temperature to calculate isentropic flow conditions at the nozzle throat.

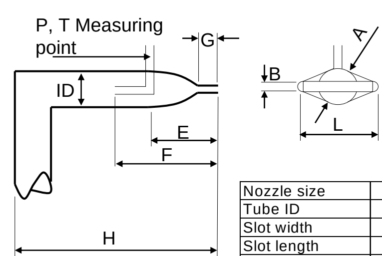

Nozzle size	A	12.5	20	40
Tube ID	ID	10	18	38
Slot width	B	0.3	4	4
Slot length	L	15.5	29.5	57
Dh	Dh	0.6	3.9	7.6
Radius start	E	30	45	70
Sample point	F	50	65	85
Slot land	G	4	4	8
Overall length	H	190	150	150

*dimensions in mm

Figure 3: Nozzle design parameters

Results and Discussion

An ANOVA analysis of the factorial experiment showed the factors; isentropic Reynolds number

(Re_{isen}), nozzle angle (α), nozzle size and distance from the sidewall (s/Dh) as having a statistically significant effect (at the 5% level) on the mean grid sidewall temperature ($T_{avg\ grid}$); each nozzle arrangement factor is discussed in further detail below.

Isentropic Reynolds Number

The effect of isentropic Reynolds number (Re_{isen}) on $T_{avg\ grid}$ for the three nozzle sizes at two s/Dh distances is shown in Figure 4. Increasing Re_{isen} reduced $T_{avg\ grid}$ for all nozzle sizes with the rate of temperature reduction greatest at low Re_{isen} values. The 20mm and 40mm nozzle sizes show similar behaviour in the low Re_{isen} range when s/Dh = 10 or 20. The high pressure nozzle (12.5mm) had a more significant temperature reduction with increasing s/Dh and a reduced rate of temperature reduction with increasing Re_{isen}. The observed effect is consistent with the literature [3-8]

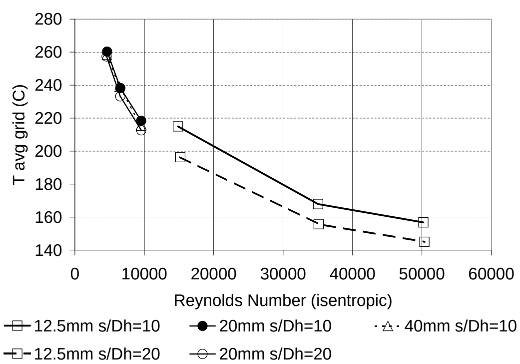

Figure 4: Effect of Re_{isen} on $T_{avg\ grid}$ for 12.5mm and 20mm nozzles with s/Dh =10 and 20, 40mm nozzle s/Dh=10, $\alpha = 90°$

Nozzle impingement angle

The effect of nozzle impingement angle (α) on the vertical thermal profile of the sidewall is shown in Figure 5 for the 12.5mm size nozzle at Re_{isen} = 15,000. Similar trends were observed for the 20 and 40mm nozzle sizes also. Nozzle angle affected the top, bottom and peak sidewall temperatures. A 90° nozzle angle produced the lowest peak temperature and significantly cooled the top and bottom sidewall regions. A nozzle angle of 45° resulted in significant bottom sidewall cooling with only moderate cooling at the top. This arrangement is useful if the sidewall to anode crust is hard and lower sidewall cooling is required. A nozzle angle of 135° resulted in minimal temperature reduction with the majority of cooling occurring at the top of the sidewall.

The effect of nozzle angle on $T_{avg\ grid}$ was explored. For all nozzles, the lowest $T_{avg\ grid}$ was at a nozzle angle of 90° with the next lowest temperature at 45°. Larger nozzle to sidewall distance (s/Dh) had a greater nozzle angle effect especially for the 12.5mm size nozzle. A 90° nozzle angle provides the most effective overall sidewall cooling.

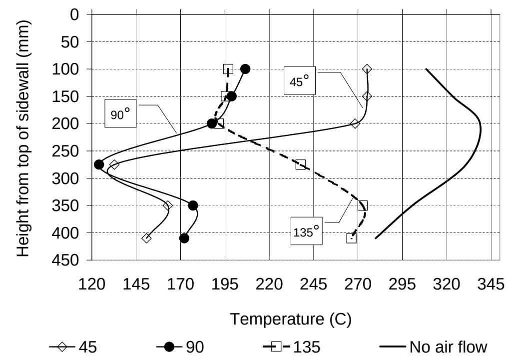

Figure 5: Effect of nozzle angle (α) on vertical centreline sidewall temperature profile for 12.5mm nozzle, s/Dh = 20, Re_{isen} = 15,000

Nozzle distance from sidewall

The effect of dimensionless sidewall distance (s/Dh) on the vertical sidewall temperature profile for the 20mm size nozzle at 90° is shown in Figure 6. Increasing s/Dh ,up to approximately s/Dh = 15, resulted in reduced sidewall temperatures and a flatter thermal profile, especially at the impingement point. At s/Dh=25, sidewall temperatures were generally higher than that at s/Dh=15.

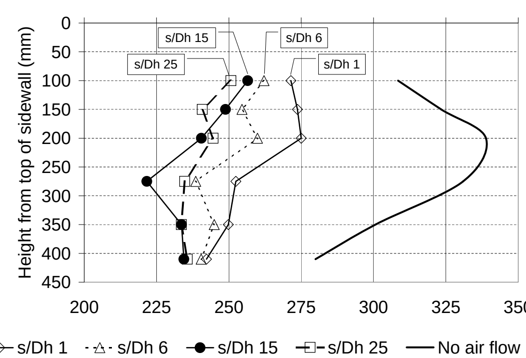

Figure 6: Effect of nozzle to sidewall distance (s/Dh) on the vertical centreline thermal profile of sidewall for 20mm size nozzle, Re_{isen} = 6500, $\alpha = 90°$

The effect of nozzle distance (s/Dh) on $T_{avg\ grid}$ is shown in Figure 7. The 12.5 and 20mm nozzle sizes showed reduced mean sidewall temperatures with increasing s/Dh distance in the range tested. The 40mm nozzle size showed maximum temperature reduction when s/Dh ≈ 6 after which sidewall temperatures increased.

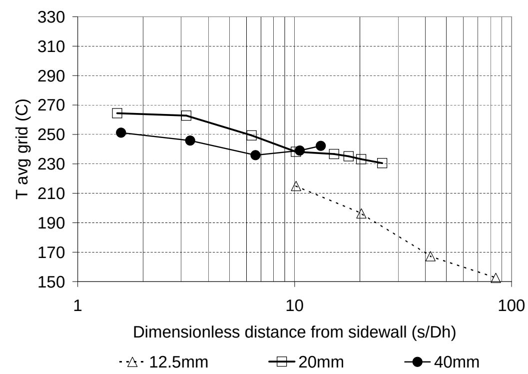

Figure 7: Effect of nozzle distance (s/Dh) on $T_{avg\ grid}$, $\alpha = 90°$, 12.5mm-Re_{isen} = 15,000, 20mm and 40mm-Re_{isen} = 6500

The effect of s/Dh on the stagnation overall heat transfer coefficient ($U_{stag\ isen}$), which includes thermal radiation, for the 12.5, 20 and 40mm nozzles is shown in Figure 8. $U_{stag\ isen}$ reduces with s/Dh distance for the 12.5 and 40mm nozzles however the 20mm nozzle has a local peak at s/Dh ≈ 6; the 12.5mm nozzle does not have results s/Dh < 10 hence a local peak less than this cannot be identified. The 20mm nozzle arrangement agrees with Martin's [3] Nu_{stag} which has a local peak at s/Dh ≈ 6-8 and with Goldstein et al's [7] peak Nu_{stag} occurring at s/Dh = 8 for a round nozzle. Beitelmal et al's [4, 5] Nu_{stag} decreases with s/Dh and has no local peak which agrees with the 40mm nozzle results.

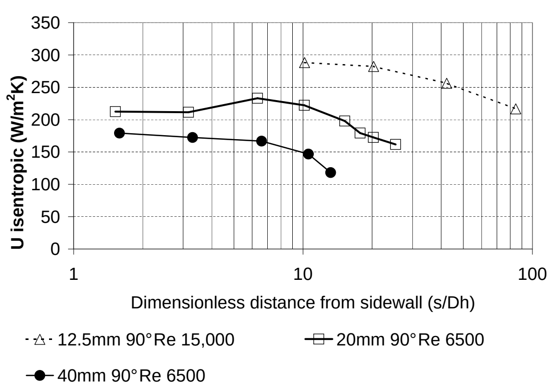

Figure 8: Effect of nozzle distance on stagnation overall heat transfer coefficient ($U_{stag\ isen}$)based on nozzle throat temperature,12.5mm - Re_{isen} = 15,000, 20mm and 40mm - Re_{isen} = 6500, $\alpha = 90°$

At locations furthest from the centre line (TE17, 27, 12, 26, 37, 13), the wider 40mm nozzle at fixed s/Dh and Re_{isen}, had the lowest temperatures which in turn resulted in low $T_{avg\ grid}$ values, it also had the lowest $U_{stag\ isen}$ hence the heat transfer coefficient in the stagnation region does not necessarily reflect $T_{avg\ grid}$ however a relationship with nozzle width (slot length) exists.

Ambient air entrapment of a small slot nozzle impinging on a large surface will resemble that of a single round nozzle (in contrast to that of a full width slot nozzle found in [3, 5, 4]). Goldstein et al's [7] round nozzle work identified a local maximum Nu_{stag} and related it to turbulent mixing of air from the shear layer; subsequent reduction in stagnation Nu_{stag} with increasing s/Dh was assigned to reduced jet arrival velocity. At fixed Re_{isen}, the 40mm nozzle exit velocity is half that of the 20mm nozzle which could have reduced turbulent mixing at the stagnation point thus preventing the local maximum $U_{stag\ isen}$ when compared with the 20mm nozzle. This may also explain the difference in Beitelmal et al's [4, 5] correlation, based on low nozzle throat velocity, compared to Martin's [3] more general, higher velocity, correlation.

Air Power

$T_{avg\ grid}$ verses air power is shown in Figure 9 for a nozzle angle of 90°. The no air flow case provides a comparison of the cooling achieved. The air power

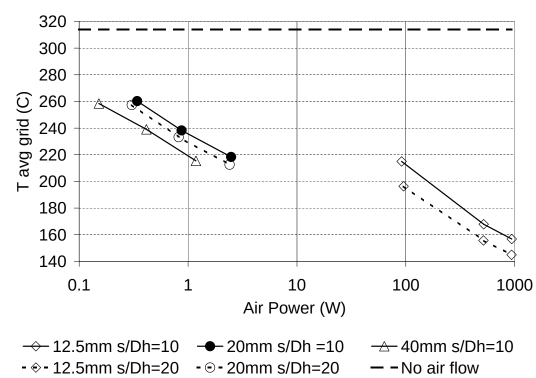

Figure 9: $T_{avg\ grid}$ verses air power (W), $\alpha = 90°$, 12.5 and 20mm nozzles s/Dh = 10 and 20, for 40mm nozzle s/Dh = 10

scale is logarithmic showing the significantly higher energy requirement of the high pressure nozzle. At a sidewall temperature of approximately 215°C the 20mm and 40mm size nozzles have an air power requirement of 1 to 2.5 W compared to approximately 90 W for the high pressure, 12.5mm size nozzle at s/Dh = 10. At s/Dh = 20 the high pressure nozzle has a lower sidewall temperature than the 20mm nozzle. The 40mm nozzle also has a lower air power requirement for similar cooling potential as the 20mm size nozzle at s/Dh =10 indicating a larger, low pressure, nozzle is more effective. Figure 9 indicates that small, high pressure, nozzles are not energy efficient for moderate sidewall cooling of wide sidewall areas at low nozzle to wall distances (s/Dh) however they do have high cooling capability at larger s/Dh values.

Conclusions

Isentropic Reynolds number (Re_{isen}), nozzle angle (α), nozzle size and dimensionless distance from sidewall (s/Dh) effect the sidewall cooling capability of compressed air nozzles at high and low pressures.

Increasing Re_{isen} reduces sidewall temperatures for all nozzle sizes tested. The greatest rate of temperature reduction occurred at low Re_{isen} with large, low pressure nozzles.

90° nozzle angles have the largest mean sidewall temperature reduction. 45° nozzle angles cool the lower sidewall regions whilst providing moderate cooling at the sidewall top. 135° nozzle angles significantly cool the top sidewall with moderate cooling at the peak temperature location and lower sidewall.

Nozzle to sidewall distance (s/Dh) has a significant effect on sidewall cooling with the optimum s/Dh depending on the combination of nozzle arrangement factors including nozzle size and nozzle exit velocity. The largest mean sidewall temperature reduction occurred in the range of s/Dh = 6-15. The stagnation overall heat transfer coefficient $U_{stag\ isen}$ reduces with increasing s/Dh for the 12.5 and 40mm nozzles. $U_{stag\ isen}$ is localised and is not a direct indicator of mean overall sidewall cooling.

Small, high pressure nozzles, require significantly more energy than larger, low pressure nozzles, for equivalent mean sidewall cooling levels in the ranges tested. The most effective nozzle arrangement for moderate cooling of a wide portion of the sidewall was a low pressure, 40mm nozzle, at an angle of 90° and s/Dh = 6-10.

Nomenclature

B = slot width (mm)
L = slot length (mm)
Dh = nozzle hydraulic diameter
s = distance from wall to end of nozzle (mm)
x = distance along the wall from the stagnation point (mm)
α = inclination angle (degrees)
q = heat flux measurement (XE2) (W/m^2)
$U_{stag\ isen}$ = stagnation overall heat transfer coefficient (W/m^2K)
Nu = Nusselt number
Re_{isen} = Reynolds number = $\frac{uDh}{\nu}$
u = nozzle velocity (m/s)
ν = kinematic viscosity
γ = index for air $\frac{Cp}{Cv}$
P = stagnation pressure (absolute) (Pa)
T = stagnation temperature (absolute) (K)
R = specific gas constant = 287.04 (J/kgK)

subscripts

$_o$ = stagnation upstream of nozzle exit
$_{throat}$ = throat conditions
$_{choked}$ = nozzle choked
$_{unchoked}$ = nozzle un choked
$_{isen}$ = isentropic flow assumed
$_{stag}$ = stagnation region
$_w$ = wall
$_{ambient}$ = ambient air conditions

Acknowledgements

Financial support from Rio Tinto Aluminium Technology and The University of Auckland is gratefully acknowledged. I would also like to thank Eng Fui Siew (LMRC), Dr Arden Miller (Statistics Dept - University of Auckland) and Trevor White (Engineering Workshop - University of Auckland) for assistance with experimental work.

References

[1] J. Bos, B. Feve, and P. Homsi. Electrolytic pot for the production of aluminium using the hall-heroult process comprising cooling means, 2001. US 6,251,237 B1.

[2] J. P. Quayle, editor. *Kempes Engineers Year Book 1987 (section F)*. Morgan Crampion, 1987.

[3] H. Martin. Heat and mass transfer between impinging gas jets and solid surfaces. In *Advances in Heat Transfer*, volume 13, pages 1–60. Academic Press, New York, 1977.

[4] A. H. Beitelmal, A. J. Shah, and M. A. Saad. Analysis of an impinging two-dimensional jet. *Journal of Heat Transfer, Transactions ASME*, 128(March 2006):307–310, 2006.

[5] A. H. Beitelmal, M. A. Saad, and C.D. Patel. The effect of inclination on the heat transfer between a flat surface and an impinging two-dimensional air jet. *International Journal of Heat and Fluid Flow*, 21(2):156–163, 2000.

[6] K. Jambunathan, E. Lai, M. A. Moss, and B. L. Button. A review of heat transfer data for single circular jet impingement. *International Journal of Heat and Fluid Flow*, 13(2):106–115, 1992.

[7] R. J. Goldstein, A. I. Behbahani, and K. Kieger Heppelmann. Streamwise distribution of the recovery factor and the local heat transfer coefficient to an impinging circular air jet. *International Journal of Heat and Mass Transfer*, 29(8):1227–1235, 1986.

[8] R. J. Goldstein and A. I. Behbahani. Impingement of a circular jet with and without cross flow. *International Journal of Heat and Mass Transfer*, 25(9):1377–1382, 1982.

[9] M. J. Zucrow and J. D. Hoffman. *Gas Dynamics*, volume 1. John Wiley & Sons, New York, 1976.